Removal of Shelterin Reveals the Telomere End-Protection Problem

Agnel Sfeir and Titia de Lange

Science **336**, 593 (2012);
DOI: 10.1126/science.1218498

Removal of Shelterin Reveals the Telomere End-Protection Problem

Agnel Sfeir* and Titia de Lange†

The telomere end-protection problem is defined by the aggregate of DNA damage signaling and repair pathways that require repression at telomeres. To define the end-protection problem, we removed the whole shelterin complex from mouse telomeres through conditional deletion of TRF1 and TRF2 in nonhomologous end-joining (NHEJ) deficient cells. The data reveal two DNA damage response pathways not previously observed upon deletion of individual shelterin proteins. The shelterin-free telomeres are processed by microhomology-mediated alternative-NHEJ when Ku70/80 is absent and are attacked by nucleolytic degradation in the absence of 53BP1. The data establish that the end-protection problem is specified by six pathways [ATM (ataxia telangiectasia mutated) and ATR (ataxia telangiectasia and Rad3 related) signaling, classical-NHEJ, alt-NHEJ, homologous recombination, and resection] and show how shelterin acts with general DNA damage response factors to solve this problem.

Aspects of the end-protection problem have been revealed in yeast, plant, and mammalian cells based on adverse events at telomeres lacking certain telomeric proteins (*1*). However, the fate of telomeres devoid of all protective factors is unknown, and hence the end-protection problem remained undefined. Mammals solve the end-protection problem through the agency of shelterin (*2*), a multisubunit protein complex anchored onto duplex telomeric DNA by the TTAGGG repeat binding factors TRF1 and TRF2 (fig. S1). Both TRF1 and TRF2 interact with TIN2 (TRF1-interacting nuclear factor 2), which in turn links the heterodimer formed by TPP1 (TINT1/PTOP1/PIP1) and POT1 (protection of telomeres 1; POT1a and POT1b in mouse) to telomeres. TPP1/POT1 interacts with the single-stranded TTAGGG repeats present at mammalian chromosome ends in the form of a

Laboratory for Cell Biology and Genetics, The Rockefeller University, 1230 York Avenue, New York, NY 10065, USA.

*Present address: Developmental Genetics Program and Department of Cell Biology, Skirball Institute, New York University School of Medicine, New York, NY 10016, USA.
†To whom correspondence should be addressed. E-mail: delange@mail.rockefeller.edu

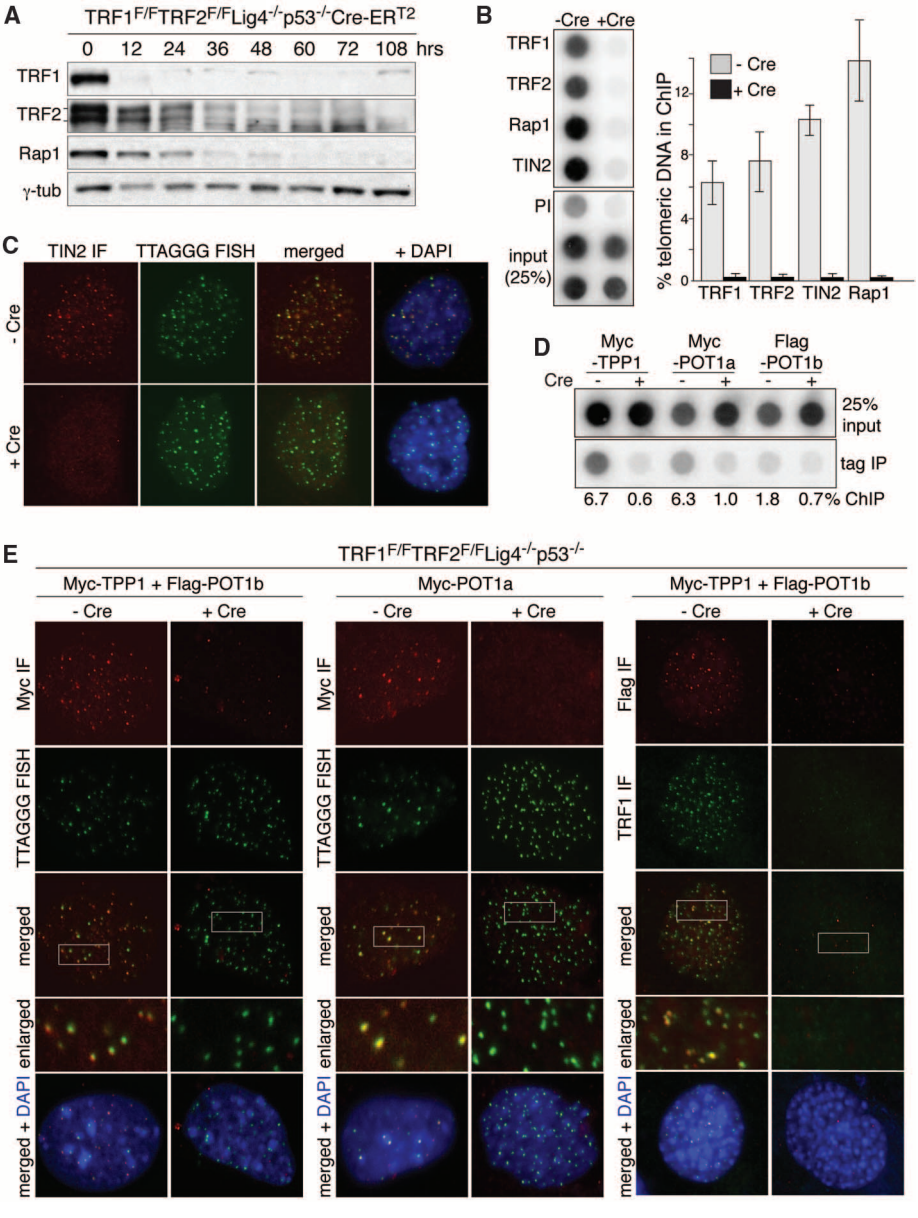

Fig. 1. Shelterin-free telomeres. (**A**) Immunoblots for TRF1, TRF2, and Rap1 after 4-OHT–induced TRF1/2 DKO from Lig4$^{-/-}$p53$^{-/-}$Cre-ERT2 MEFs. (**B**) ChIP for telomeric DNA associated with shelterin proteins in TRF1$^{F/F}$TRF2$^{F/F}$p53$^{-/-}$Lig4$^{-/-}$ MEFs (day 5 after H&R-Cre). Bars average percentage of telomeric DNA recovered in two independent experiments, ± SEMs. (**C**) IF-FISH for TIN2 at telomeres in TRF1$^{F/F}$TRF2$^{F/F}$p53$^{-/-}$Lig4$^{-/-}$ MEFs day 5 after H&R-Cre. TIN2 IF (red); telomeric PNA probe [fluorescein isothiocyanate (FITC), green]. (**D**) ChIP for telomeric DNA associated with Myc-TPP1, Myc-POT1a, and Flag-POT1b in TRF1$^{F/F}$TRF2$^{F/F}$p53$^{-/-}$ Lig4$^{-/-}$ cells, with (+) and without (–) H&R-Cre. (**E**) IF for the telomeric localization of Myc-TPP1, Myc-POT1a, and Flag-POT1b (red, MYC or Flag antibodies) in TRF1$^{F/F}$TRF2$^{F/F}$p53$^{-/-}$Lig4$^{-/-}$ MEFs (5 days after H&R-Cre). Green, telomeric PNA probe or TRF1 IF.

50 to 400 nucleotide (nt) 3′ overhang. The sixth shelterin subunit, Rap1, is a TRF2-interacting factor. Deletion of each of the individual shelterin proteins revealed that the end-protection problem minimally involves the repression of ATM (ataxia telangiectasia mutated) and ATR (ataxia telangiectasia and Rad3 related) signaling as well as inhibition of double-strand break (DSB) repair by nonhomologous end-joining (NHEJ) and homology-directed repair (HDR). However, the possibility of redundant repression of additional DNA damage response (DDR) pathways has prevented a definitive description of the end-protection problem in mammalian cells.

We sought to finalize the tally of telomere-threatening pathways by generating telomeres devoid of all shelterin proteins and their associated factors. We set out to remove both TRF1 and TRF2, which is predicted to lead to complete loss of shelterin (fig. S1). In this TRF1/2 double-knockout (DKO), NHEJ of telomeres devoid of TRF2 thwarts detection of potential novel pathways acting on deprotected chromosome ends. We therefore created conditional TRF1/2 DKO mouse embryo fibroblasts (MEFs) with additional deficiencies in DNA ligase IV (Lig4), Ku80, or 53BP1, which are predicted to minimize telomere fusion (*3*–*5*). Cre was expressed from a self-deleting Hit-and-Run (H&R-Cre) retrovirus or from a genetically introduced tamoxifen (4-OHT)–inducible Cre (Cre-ERT2 in the Rosa26 locus). $TRF1^{F/F}TRF2^{F/F}Lig4^{-/-}p53^{-/-}$Cre-ERT2 MEFs rapidly lost TRF1, TRF2, and Rap1 when treated with 4-OHT and telomeric chromatin immunoprecipitation (ChIP) and immunofluorescence (IF) established that TRF1, TRF2, Rap1, and TIN2 disappeared from telomeres (Fig. 1, A to C). Furthermore, using tagged alleles to facilitate analysis, IF and ChIP documented loss of TPP1 and POT1a/b from the telomeres (Fig. 1, D and E, and fig. S2, A and B). Thus, the TRF1/2 DKO generates shelterin-free telomeres. However, the telomeric DNA remained packaged in nucleosomal chromatin (fig. S2C).

As expected from the ATM/ATR signaling elicited by removal of TRF2 and POT1a, respectively (*6*), cells with shelterin-free telomeres showed phosphorylation of Chk2 and Chk1,

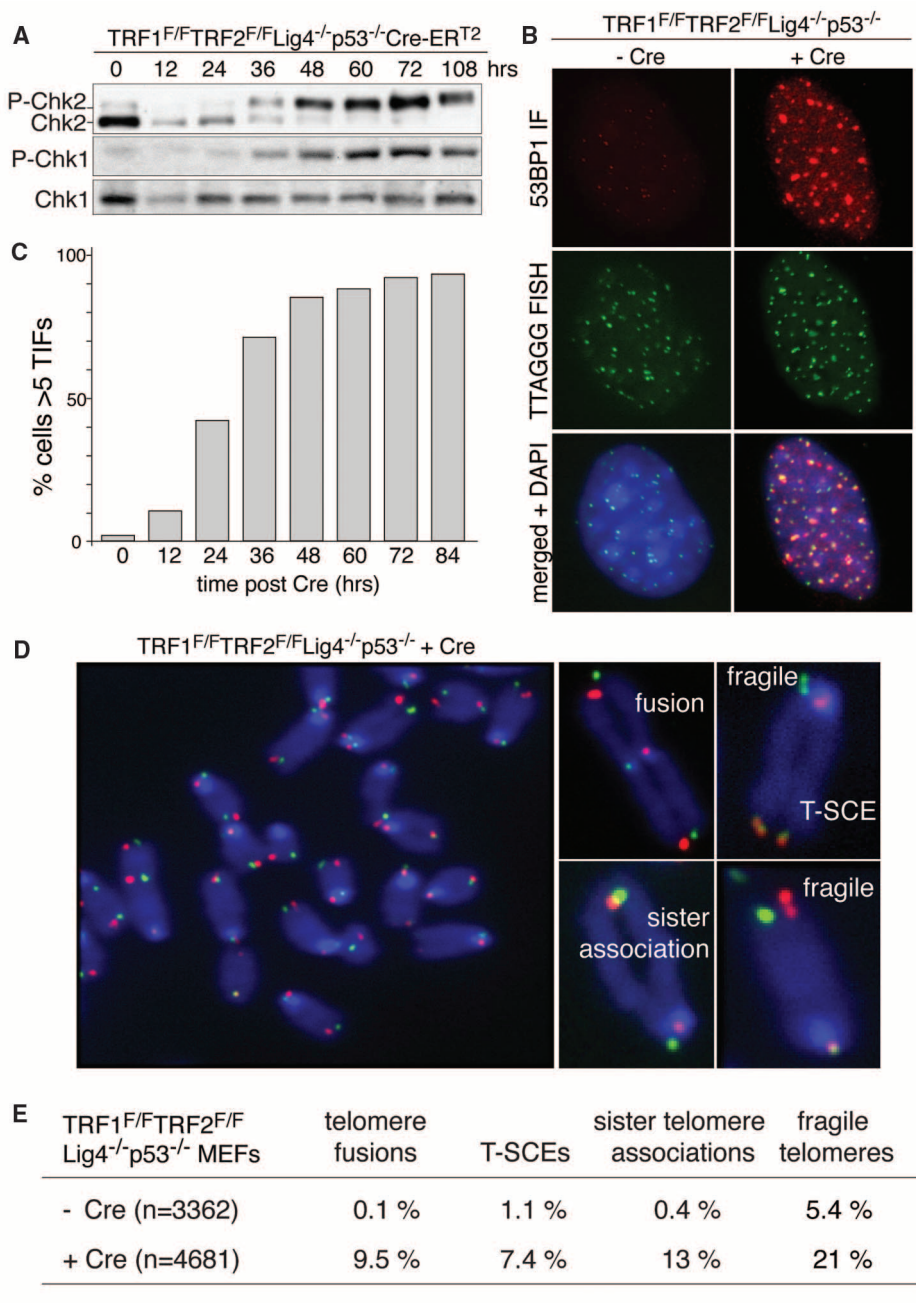

Fig. 2. Telomere dysfunction upon shelterin loss. (**A**) Induction of P-Chk1 and P-Chk2 after TRF1/2 codeletion. (**B**) IF-FISH assay for TIFs (telomere dysfunction-induced foci) in $TRF1^{F/F}TRF2^{F/F}Lig4^{-/-}p53^{-/-}$Cre-ERT2 MEFs (5 days after Cre). FISH for telomeres (green), IF for 53BP1 (red), and 4′,6-diamidino-2-phenylindole (DAPI) as DNA counterstain (blue). (**C**) Time course of TIF response as in (B). TIFs were scored in $TRF1^{F/F}TRF2^{F/F}Lig4^{-/-}p53^{-/-}$Cre-ERT2 cells at the indicated time points after 4-OHT. Cells with ≥5 telomeric 53BP1 foci were scored as TIF positive (n > 100 nuclei per time point). (**D**) Metaphase spread from $TRF1^{F/F}TRF2^{F/F}Lig4^{-/-}$ $p53^{-/-}$ cells at 108 hours after Cre treatment, analyzed by telomeric CO-FISH using a FITC-OO-$[CCCTAA]_3$ PNA probe (green) and a Tamra-OO-$[TTAGGG]_3$ PNA probe (red). Blue, DAPI. Examples of fragile telomeres, chromosome- and chromatid-type fusions, sister telomere associations, and T-SCEs are on the right. (**E**) Quantification of aberrant telomeres in Cre-treated $TRF1^{F/F}TRF2^{F/F}Lig4^{-/-}p53^{-/-}$ MEFs analyzed as in (D).

accumulated telomeric 53BP1 foci, and underwent polyploidization (Fig. 2, A to C, and fig. S2, D and E). Telomeric chromosome-orientation fluorescence in situ hybridization (CO-FISH) revealed a cornucopia of telomeric aberrations in metaphase spreads (Fig. 2, D and E). Telomeres often displayed the fragile telomere phenotype typical of the replication defect induced by TRF1 loss (*7*, *8*). There were frequent sister telomere associations, which were previously noted in cells lacking TRF1, TIN2, TPP1, or POT1a/b (*7*, *9*–*11*), and ~7.5% of the telomeres showed sequence exchanges between sister telomeres [telomere sister chromatid exchanges (T-SCEs)], indicative of the HDR activated upon loss of either Rap1 or POT1a/b (*12*, *13*).

Because these Lig4 cells were NHEJ deficient, it was unexpected that nearly 10% of the telomeres became fused (Fig. 2E and Fig. 3). Furthermore, TRF1/2 DKO in Ku80-deficient MEFs resulted in fusions involving 65% of telomeres (Fig. 3, A and B, and fig. S3A). These results suggested that the shelterin-free telomeres are processed by alt-NHEJ, which is repressed by Ku70/80 and, to a lesser extent, by Lig4 (*14*–*18*). Consistent with alt-NHEJ, which is known to be promoted by poly (adenosine diphosphate ribose) polymerase 1 (PARP1) (*16*, *19*), repression of PARP1 with a short hairpin RNA (shRNA) or olaparib (*20*) significantly reduced the fusion of shelterin-free telomeres in Ku-deficient cells (Fig. 3C and fig. S3B). ShRNA knockdown also implicated Lig3 in the alt-NHEJ of telomeres (Fig. 3D and fig. S3C), pointing to microhomology-mediated end-joining (*21*), possibly facilitated by the 2 A-T base pairs per telomeric repeat in annealing 3′ overhangs. Analysis of G0-arrested cells revealed that the alt-NHEJ pathway also operates in nonproliferating cells (Fig. 3E and fig. S3, D and E). Although most telomeres were processed by alt-NHEJ when shelterin was removed in toto, individual deletion of shelterin components from Ku null cells failed to result in frequent telomere fusions (Fig. 3F). The finding that deletion of TPP1 does not elicit alt-NHEJ at telomeres in Ku null cells (Fig. 3F) contrasts with a previous suggestion that TPP1/POT1a/b are required to repress alt-NHEJ at telomeres (*15*). Possibly, the different method used to remove TPP1/POT1a/b in that study had additional effects. We conclude that Lig3/PARP1-dependent alt-NHEJ, is blocked by multiple shelterin components (or their interacting factors) as well as Ku70/80 (Fig. 3G).

We anticipated that fully deprotected, unfused telomeres would be subject to nucleolytic degradation, which is a marked outcome of telomere dysfunction in yeast [reviewed in (*1*)]. However, there was no evidence for overt nucleolytic processing of the shelterin-free telomeres (fig. S4A). In addition, in the absence of Ku70/80, which represses resection at telomeres in other eukaryotes (*22*–*25*), the overhang signal at the shelterin-free telomeres increased by a factor of <3, even when telomere fusions were repressed by inhibiting PARP1 (fig. S4, A to E).

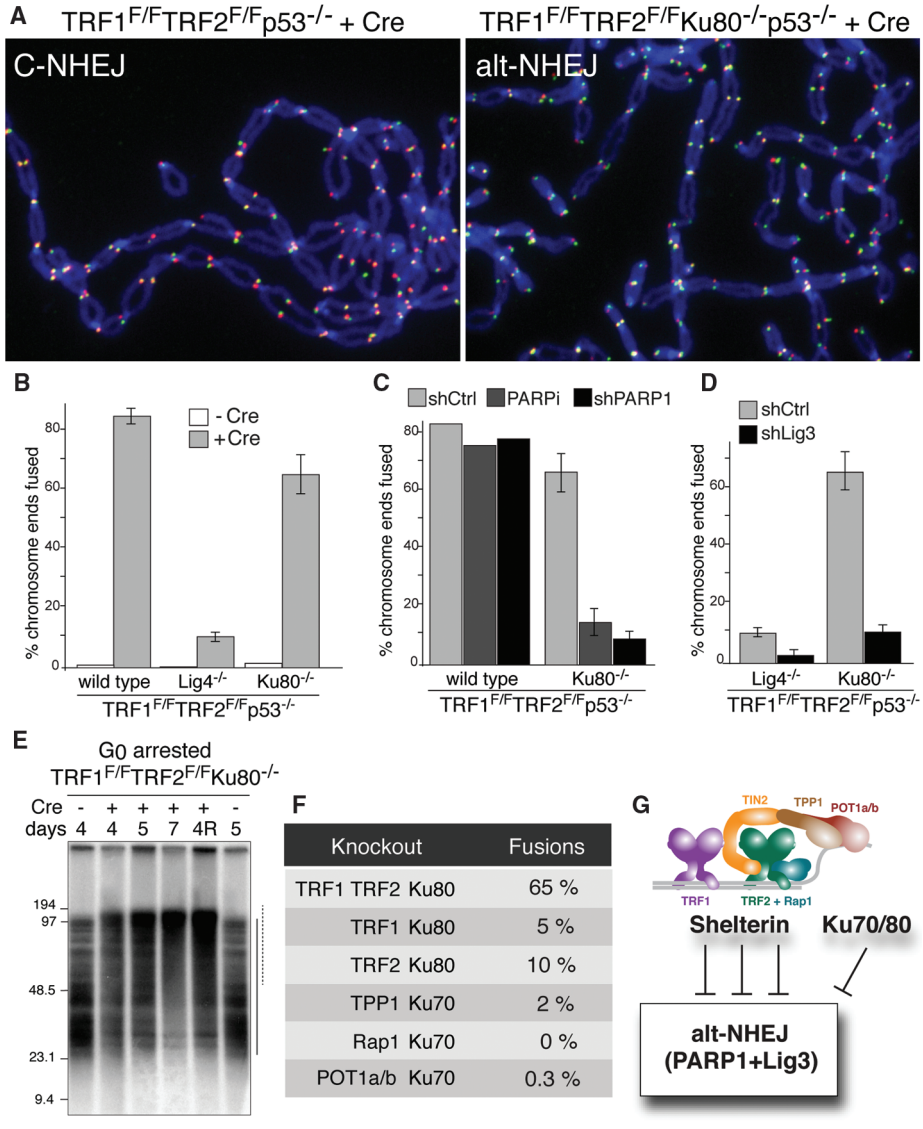

Fig. 3. Lig3- and PARP1-dependent alt-NHEJ in the absence of shelterin. (**A**) Metaphase chromosomes of the indicated MEFs analyzed (as in Fig. 2D) at 108 hours after Cre. (**B**) Quantification of telomere fusions in the indicated MEFs at 108 hours after H&R-Cre. Bars and not error bars means of three independent experiments, ± SDs. (**C**) Quantification of telomere fusions induced by deleting TRF1 and TRF2 [as in (A)] after treatment with PARP1 shRNA or 0.5 μM olaparib. (**D**) Quantification of telomere fusions [as in (**C**)] in cells treated with Lig3 or control shRNA. (**E**) Alt-NHEJ in G0 arrested TRF1$^{F/F}$TRF2$^{F/F}$Ku80$^{-/-}$p53+/+Cre-ERT2 MEFs. *Mbo*I and *Alu*I digested DNA resolved on a pulsed-field gel electrophoresis probed with end-labeled [AACCCT]$_4$. Dashed and solid lines: fused and unfused telomeres, respectively. Day 4R: cells released on day 4 and analyzed on day 5. (**F**) Percentage of fused telomeres in Ku-deficient MEFs lacking the indicated shelterin subunit(s). Cells were analyzed at 108 hours after Cre-mediated deletion of the floxed alleles of shelterin. (**G**) Summary of the repression of Lig3- and PARP1-dependent alt-NHEJ by shelterin and Ku70/80.

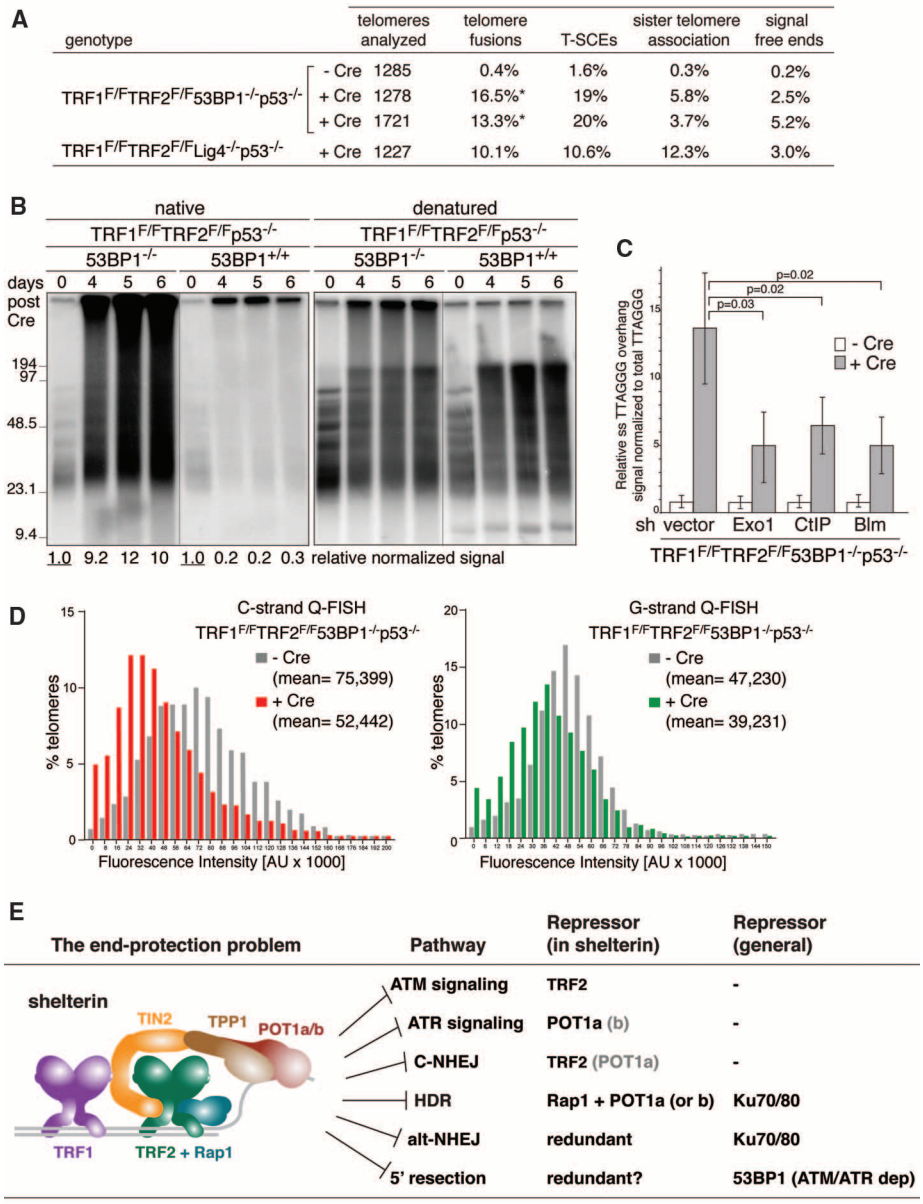

Fig. 4. 53BP1 blocks 5′ end resection and shortening of shelterin-free telomeres. (**A**) Quantification of telomere aberrations in Cre-treated (108 hours) TRF1$^{F/F}$TRF2$^{F/F}$53BP1$^{-/-}$ p53$^{-/-}$ and TRF1$^{F/F}$TRF2$^{F/F}$Lig4$^{-/-}$p53$^{-/-}$ MEFs. *, 93% of the cells had ~12% of chromosome ends fused, whereas 7% of the cells had more than 50% of the chromosome ends fused. (**B**) Representative in-gel 3′ overhang analysis of the indicated MEFs after Cre treatment. Relative overhang signals were normalized to total telomeric DNA (lanes without Cre set to 1). (**C**) Quantification of 3′ overhangs of TRF1$^{F/F}$TRF2$^{F/F}$53BP1$^{-/-}$p53$^{-/-}$ MEFs (+ or − H&R-Cre, 108 hours) treated with Exo1, CtIP, and Blm shRNAs. The ss/total signal ratios of the +Cre samples are expressed relative to the −Cre samples for each shRNA treatment. Means of three independent experiments ± SDs. *P* values: two-tailed student's *t* tests. (**D**) Q-FISH of telomeres in TRF1$^{F/F}$ TRF2$^{F/F}$53BP1$^{-/-}$p53$^{-/-}$ MEFs with or without H&R-Cre (day 5). (**E**) Summary of the end-protection problem.

This modest effect suggested that Ku70/80 does not play a major role in repressing 5′ end resection.

It was recently shown that 5′ end resection at DSBs is minimized by 53BP1, a DDR factor that binds near DSBs and at dysfunctional telomeres in response to ATM or ATR signaling (*26*, *27*). To test the role of 53BP1 at shelterin-free telomeres, we generated TRF1$^{F/F}$TRF2$^{F/F}$53BP1$^{-/-}$p53$^{-/-}$ MEFs. Neither classical nor alt-NHEJ is anticipated at the shelterin-free telomeres of these cells, because 53BP1 is required for Lig4-dependent telomere fusions (*5*) and Ku70/80 impedes alt-NHEJ (Fig. 3). Indeed, TRF1/2 DKO in 53BP1 null cells elicited a modest level of telomere fusions, mediated mainly by Lig3 (Fig. 4A and fig. S5, A and B), and infrequent sister telomere associations (Fig. 4A). The telomeric overhang signal increased by a factor of ~10 after the TRF1/2 DKO, but not when either TRF1 or TRF2 were deleted from 53BP1-deficient cells (Fig. 4, B and C, and fig. S5C). The excessive signal was due to single-stranded DNA at a 3′ end, as it was removed by the *Escherichia coli* 3′ exonuclease Exo1 (fig. S5D). The increase in the overhang signal was maximal in cycling cells, regardless of the cell cycle phase, but also occurred in G0 arrested cells (fig. S6, A to D). Because 5′ end resection at DSBs is mediated by CtIP, Blm, and Exo1 (*28*–*30*), we examined the role of these factors by shRNA knockdown. Depletion of CtIP, Blm, or Exo1 significantly reduced the overhang signal, establishing that 5′ end resection contributes to the phenotype (Fig. 4C and fig. S7, A to E). Furthermore, quantitative FISH (Q-FISH) recorded a 20 to 30% reduction in the length of the telomeric G-rich and C-rich strands, consistent with nucleolytic degradation (Fig. 4D). Thus, telomeres are in danger of excessive 5′ end resection by enzymes involved in DSB processing. This hyperresection is blocked by shelterin and, in the absence of shelterin, by 53BP1 (Fig. 4E and fig. S7F).

The deleterious events at shelterin-free telomeres revealed that six pathways define the end-protection problem (Fig. 4E). Shelterin is the main armor of chromosome ends, providing protection against classical NHEJ and inadvertent activation of the ATM and ATR signaling. In addition to these primary threats, telomeres can fall victim to alt-NHEJ, HDR, and unmitigated resection. However, these pathways are also blocked by either Ku70/80 or 53BP1, providing a second layer of defense. Although 53BP1 can minimize hyperresection, it will only do so at telomeres that elicit a DNA damage signal. Therefore, the protective ability of 53BP1 is limited and shelterin must prevent hyperresection under most conditions. We speculate that the mechanism by which shelterin fulfills this task is related to how it governs the formation of the correct telomeric overhangs after DNA replication. In contrast to 53BP1, Ku70/80 should be available to blocks alt-NHEJ and HDR at telomeres independent of a DNA damage signal. Why, then, should shelterin also repress these pathways? The redundancy may ensure greater protection, or the repression of alt-NHEJ and HDR may be a secondary outcome of the mechanism by which shelterin executes one of its other functions. As the genetic deconstruction of telomeres has illuminated the full spectrum of processing reactions that threaten chromosome ends lacking proper protection, this study provides a framework for the understanding of the consequences of telomere dysfunction arising from telomere attrition in aging and cancer.

References and Notes

1. T. de Lange, *Science* **326**, 948 (2009).
2. W. Palm, T. de Lange, *Annu. Rev. Genet.* **42**, 301 (2008).
3. G. B. Celli, T. de Lange, *Nat. Cell Biol.* **7**, 712 (2005).
4. G. B. Celli, E. L. Denchi, T. de Lange, *Nat. Cell Biol.* **8**, 885 (2006).

5. N. Dimitrova, Y. C. Chen, D. L. Spector, T. de Lange, *Nature* **456**, 524 (2008).
6. E. L. Denchi, T. de Lange, *Nature* **448**, 1068 (2007).
7. A. Sfeir *et al.*, *Cell* **138**, 90 (2009).
8. P. Martínez *et al.*, *Genes Dev.* **23**, 2060 (2009).
9. K. K. Takai, T. Kibe, J. R. Donigian, D. Frescas, T. de Lange, *Mol. Cell* **44**, 647 (2011).
10. T. Kibe, G. A. Osawa, C. E. Keegan, T. de Lange, *Mol. Cell. Biol.* **30**, 1059 (2010).
11. D. Hockemeyer, J. P. Daniels, H. Takai, T. de Lange, *Cell* **126**, 63 (2006).
12. A. Sfeir, *Science* **327**, 1657 (2010).
13. W. Palm, D. Hockemeyer, T. Kibe, T. de Lange, *Mol. Cell. Biol.* **29**, 471 (2009).
14. C. Boboila *et al.*, *J. Exp. Med.* **207**, 417 (2010).
15. R. Rai *et al.*, *EMBO J.* **29**, 2598 (2010).
16. M. Wang *et al.*, *Nucleic Acids Res.* **34**, 6170 (2006).
17. D. Simsek, M. Jasin, *Nat. Struct. Mol. Biol.* **17**, 410 (2010).
18. C. T. Yan *et al.*, *Nature* **449**, 478 (2007).
19. W. Y. Mansour, T. Rhein, J. Dahm-Daphi, *Nucleic Acids Res.* **38**, 6065 (2010).
20. K. A. Menear *et al.*, *J. Med. Chem.* **51**, 6581 (2008).
21. D. Simsek *et al.*, *PLoS Genet.* **7**, e1002080 (2011).
22. P. Baumann, T. R. Cech, *Mol. Biol. Cell* **11**, 3265 (2000).
23. S. Gravel, M. Larrivée, P. Labrecque, R. J. Wellinger, *Science* **280**, 741 (1998).
24. R. M. Polotnianka, J. Li, A. J. Lustig, *Curr. Biol.* **8**, 831 (1998).
25. K. Riha, D. E. Shippen, *Proc. Natl. Acad. Sci. U.S.A.* **100**, 611 (2003).
26. P. Bouwman *et al.*, *Nat. Struct. Mol. Biol.* **17**, 688 (2010).
27. S. F. Bunting *et al.*, *Cell* **141**, 243 (2010).
28. E. P. Mimitou, L. S. Symington, *Nature* **455**, 770 (2008).
29. Z. Zhu, W. H. Chung, E. Y. Shim, S. E. Lee, G. Ira, *Cell* **134**, 981 (2008).
30. S. Gravel, J. R. Chapman, C. Magill, S. P. Jackson, *Genes Dev.* **22**, 2767 (2008).

Acknowledgments: We thank D. White for exceptional dedication to the mouse husbandry involved in this project and members of the de Lange laboratory for comments on this manuscript. This work was supported by grants from the NIH to T.dL. (GM49046 and AG016642). T.dL. is an American Cancer Society Research Professor.

Supplementary Materials

www.sciencemag.org/cgi/content/full/336/6081/593/DC1
Materials and Methods
Figs. S1 to S7
References (*31*–*41*)

28 December 2011; accepted 9 March 2012
10.1126/science.1218498

Elementary Ca^{2+} Signals Through Endothelial TRPV4 Channels Regulate Vascular Function

Swapnil K. Sonkusare,[1] Adrian D. Bonev,[1] Jonathan Ledoux,[1,2] Wolfgang Liedtke,[3] Michael I. Kotlikoff,[4] Thomas J. Heppner,[1] David C. Hill-Eubanks,[1] Mark T. Nelson[1,5]*

Major features of the transcellular signaling mechanism responsible for endothelium-dependent regulation of vascular smooth muscle tone are unresolved. We identified local calcium (Ca^{2+}) signals ("sparklets") in the vascular endothelium of resistance arteries that represent Ca^{2+} influx through single TRPV4 cation channels. Gating of individual TRPV4 channels within a four-channel cluster was cooperative, with activation of as few as three channels per cell causing maximal dilation through activation of endothelial cell intermediate (IK)- and small (SK)-conductance, Ca^{2+}-sensitive potassium (K^+) channels. Endothelial-dependent muscarinic receptor signaling also acted largely through TRPV4 sparklet-mediated stimulation of IK and SK channels to promote vasodilation. These results support the concept that Ca^{2+} influx through single TRPV4 channels is leveraged by the amplifier effect of cooperative channel gating and the high Ca^{2+} sensitivity of IK and SK channels to cause vasodilation.

Endothelial cells (ECs) line all blood vessels and regulate the smooth muscle contractile state (tone). The concentration of intracellular free calcium ($[Ca^{2+}]_i$) in ECs is increased by influx and by release from intracellular stores through inositol trisphosphate receptors (IP_3Rs) in the membrane of the endoplasmic reticulum. Although Ca^{2+}-influx pathways are incompletely characterized, members of the transient receptor potential (TRP) family of nonselective cation channels have been implicated in this function. In particular, results from gene-knockout studies suggest that the vanilloid (TRPV) family member TRPV4 is involved in endothelium-dependent vascular dilation in response to flow and acetylcholine (ACh) (*1*–*5*).

Increases in endothelial $[Ca^{2+}]_i$ activate EC pathways that terminate in the release of soluble factors or initiation of processes that hyperpolarize the membrane of adjacent vascular smooth muscle cells, and thus promote dilation. These Ca^{2+}-dependent vasodilatory influences fall into three broad categories: (i) nitric oxide (NO), a tissue-permeable gas generated as a by-product of the oxidation of arginine to citrulline catalyzed by endothelial nitric oxide synthase (eNOS) (*6*); (ii) prostaglandins, produced through phospholipase A_2–dependent activation of cyclooxygenase (COX) (*7*); and (iii) endothelial-derived hyperpolarizing factor (EDHF), characterized by its strict dependence on the activity of EC intermediate-conductance (IK; $K_{Ca}3.1$) and small-conductance (SK; $K_{Ca}2.3$), Ca^{2+}-sensitive potassium (K^+) channels (*8*). Although a number of factors have been suggested as EDHF, accumulating evidence points to the importance of electrotonic spread of EC IK and/or SK channel–mediated hyperpolarizing current to smooth muscle cells through gap junctions (*8*, *9*).

Studies of Ca^{2+} signaling in ECs using conventional Ca^{2+}-binding fluorescent dyes (e.g., Fluo-4) are limited by interference from the vigorous Ca^{2+}-signaling activity of adjacent smooth muscle cells, which also readily take up such dyes. A recently developed alternative is a transgenic mouse that expresses a genetically encoded Ca^{2+} biosensor (GCaMP2) exclusively in the endothelium of the vascular wall (*10*, *11*). GCaMP2 is a fusion protein of the Ca^{2+}-binding protein calmodulin and a circularly permutated enhanced green fluorescent protein (EGFP) that fluoresces when Ca^{2+} binds to calmodulin. The GCaMP2 protein is homogeneously expressed throughout the EC (*10*) and allows long, stable recordings of intracellular Ca^{2+} in ECs in the intact blood vessel wall, without contamination of signals from smooth muscle. Using this model, we previously identified local, IP_3R-mediated Ca^{2+} events in ECs, termed Ca^{2+} pulsars (*10*), that had previously gone undetected with conventional imaging protocols.

To identify Ca^{2+}-influx pathways in the ECs of resistance arteries (i.e., arteries important in regulating peripheral resistance and blood pressure), we imaged Ca^{2+} fluorescence in isolated, small (100 μm diameter) mesenteric arteries from GCaMP2 mice using confocal microscopy (*12*). Isolated arteries were surgically opened and pinned down with the EC surface facing up (en face preparation) to improve optical resolution (*10*). In a single field of view, local Ca^{2+} signals in ~14 individual ECs could be recorded simultaneously with high spatial (0.3 μm) and temporal (15 ms) resolution. Events were analyzed offline by measuring the fluorescence intensity over time within defined 1.7-μm^2 regions of interest on images corresponding to active sites.

With IP_3R-mediated signaling eliminated by pretreatment with the sarcoplasmic reticulum/endoplasmic reticulum Ca^{2+}-ATPase (SERCA) inhibitor, cyclopiazonic acid (CPA), or the

[1]Department of Pharmacology, College of Medicine, University of Vermont, Burlington, VT 05405, USA. [2]Research Center, Montreal Heart Institute, and Department of Medicine, Université de Montréal, Montreal, QC H1T 1C8, Canada. [3]Department of Medicine and Neurobiology, and Center for Translational Neuroscience, Duke University Medical Center, Durham, NC 27710, USA. [4]Department of Biomedical Sciences, College of Veterinary Medicine, Cornell University, Ithaca, NY 14853, USA. [5]Institute of Cardiovascular Sciences, University of Manchester, Manchester M13 9NT, UK.

*To whom correspondence should be addressed. E-mail: mark.nelson@uvm.edu

Supplementary Materials for

Removal of Shelterin Reveals the Telomere End-Protection Problem

Agnel Sfeir and Titia de Lange*

*To whom correspondence should be addressed. E-mail: delange@mail.rockefeller.edu

Published 4 May 2012, *Science* **336**, 593 (2012)
DOI: 10.1126/science.1218498

This PDF file includes:

SUPPLEMENTARY MATERIALS, Sfeir and de Lange

This file includes

Material and Methods

Figs. S1-S7

References

MATERIALS AND METHODS

Derivation of MEFs and cell culture procedures

TRF1$^{F/F}$, TRF2$^{F/F}$, p53$^{-/-}$, Rosa26 Cre-ER^{T2}, Lig4$^{-/+}$, Ku80$^{-/+}$ and 53BP1$^{-/+}$ mice have been previously described (*3,7,31-35*). MEF lines were isolated from E13.5 embryos obtained by crossing TRF1$^{F/F}$TRF2$^{F/F}$Lig4$^{+/-}$p53$^{-/+}$ mice. The mice were derived after five generations of breeding of the individually targeted TRF1$^{F/F}$, TRF2$^{F/F}$, p53$^{-/-}$ and Lig4$^{+/-}$ mice. TRF1$^{F/F}$TRF2$^{F/F}$Lig4$^{+/-}$p53$^{+/+}$Cre-ER^{T2} embryos and TRF1$^{F/F}$TRF2$^{F/F}$Lig4$^{+/-}$p53$^{-/-}$ Cre-ER^{T2} embryos were isolated from crosses of TRF1$^{F/F}$TRF2$^{F/F}$Lig4$^{+/-}$p53$^{-/-}$ mice with Rosa26 Cre-ER^{T2} mice for three generations. MEF lines that were wild type for p53 were immortalized with pBabeSV40LargeT (a gift from G. Hannon). The same breeding scheme was followed to generate independent MEF lines that carried Ku80$^{-/-}$ and 53BP1$^{-/-}$ alleles instead of Lig4$^{-/-}$. Genotypes were determined by Transnetyx Inc. using real time PCR with allele-specific probes.

p53$^{-/-}$ as well as SV40LargeT-immortalized MEFs were cultured in Dulbecco's Modified Eagle Medium (DMEM) supplemented with 10-15% fetal bovine serum (FBS) (Gibco), 2 mM L-glutamine (Sigma) , 100 U/ml penicillin (Sigma), 0.1 mg/ml streptomycin (Sigma), 0.1 mM non-essential amino acids (Invitrogen), and 1 mM sodium pyruvate (Sigma). Primary MEFs, proficient for p53 were grown in media supplemented with 50 μM 2-mercaptoethanol (Chemicon). Cre recombinase was introduced by retroviral infection using Hit&Run Cre (H&R Cre) as previously described (*3*), or by treating Cre-ER^{T2} cells for 6-12 hrs with 0.5 μM 4-OH Tamoxifen (4-OHT; Sigma H7904). The t=0 time-point was set at 12 hrs after the first retroviral infection or at the time of treatment with 4-OHT. To synchronize cells in G0, primary MEFs (p53$^{+/+}$) were grown to confluency in media supplemented with 15% FBS. Serum was gradually withdrawn according to the following protocol: 15% FBS (day 1), 10% FBS (day 2), 5% FBS (day 3), 1% FBS (days 4 and 5) and 0.5% FBS (days 6 and 7). Cells were treated with 4-OHT for 6 hrs on day 8

and harvested at the indicated time points or trypsinized and re-plated in media containing 15% FBS to be released back into the cell cycle and harvested 24 hrs later. PAPR inhibition with olaparib (AZD2281; Selleck Chemicals) was carried out for 48 hrs prior to harvesting.

Lentiviral and retroviral gene delivery

shRNA treatments were carried out prior to Cre infection. shRNAs for Lig3 (pLK0.1:CCAGACTTCAAACGTCTCAAA) and PARP1 (pLK0.1:GGCCCTTGGAAACATGTATG) were introduced by 2 lentiviral infections at 12hr intervals using supernatant from transfected 293T cells. Parallel infection with pLK0.1 was used as a negative control. shRNAs for Blm (pSuperior: GGAGGGTTATTATCAAGAA and GGACCTGCTGGAAGATTTA), CtIP (pSuperior: CGAGACCTTTCTCAGTATA and GCATTAACCGGCTACGAAA) and Exo1 (pSuperior: GCATTTGGCACAAGAATTA) were introduced by 4 retroviral infections at 8 hr intervals using supernatant from transfected Phoenix cells. Parallel infection with the empty vector (pSuperior) was used as a negative control. Cells were selected for puromycin resistance for 3 days. Full-length mouse TPP1 and POT1a were cloned into pLPC-Myc puromycin retroviral vectors and POT1b was cloned into pWZL-Flag hygromycin resistant retroviral vector. The vectors were introduced into MEFs by 3 retroviral infections at 12 hr intervals using supernatant from transfected Phoenix cells. Infections were followed by puromycin selection for 3 days or hygromycin selection for 4 days.

IF and IF-FISH

Cells grown on coverslips were fixed for 5 min in 2% paraformaldehyde at room temperature and permeabilized for 5 min in 0.5% NP-40. Coverslips were incubated in blocking reagent (1 mg/ml BSA, 3% goat serum, 0.1% Triton X-100, 1 mM EDTA in PBS) for 30 min, followed by incubation with primary antibodies for 2 hrs. The antibodies used were 53BP1 (100-304A, rabbit polyclonal; Novus Biologicals); Tin2 (1447, affinity purified rabbit polyclonal), TRF1 (1449, affinity purified rabbit polyclonal), Myc (9B11, Cell Signaling), and Flag (M2, sigma). Coverslips were then washed for three times in PBS and incubated for 30 min with secondary antibodies raised against mouse or rabbit, and labeled with Alexa 488 (Molecular Probes) or Rhodamine Red-X (RRX, Jackson) respectively. Cells were then washed with PBS and the DNA was counterstained with 4.6-diamidino-2-phenylindole (DAPI). Slides were mounted with ProLong Gold antifade

(Sigma) and digital images were captured on a Zeiss Axioplan II microscope with a Hamamatsu C4742-95 camera using Improvision OpenLab software.

IF-FISH was performed as previously described (*36*) using 53BP1 primary antibody and RRX labeled secondary antibody as outlined above. After the last wash, the coverslips were fixed with 2% paraformaldehyde for 10 min at room temperature, washed three times in PBS, dehydrated consecutively in 70%, 90%, and 100% ethanol for 5 min each and allowed to air dry. FITC-OO-$[CCCTAA]_3$ labeled PNA probe (Applied Biosystems) was added in a buffer containing 70% formamide, 1 mg/ml blocking reagent (Roche), 10 mM Tris-HCl pH 7.2 and the coverslips were denatured on a heat block (5 min at 80ºC) and incubated for 4 hrs in the dark. The coverslips were washed twice with 70% formamide, 10 mM Tris-HCl pH 7.2 for 15 min each and three times in PBS for 5 min each prior to mounting and image analysis.

Western blot analysis

Cells were harvested by trypsinization, lysed in 2X Laemmli buffer (100 mM Tris-HCl pH 6.8, 200 μM DTT, 3% SDS, 20% glycerol, 0.05% bromophenol blue) at 10^4 cell/μl. The lysate was denatured for 10 min at 95ºC, and sheared by forcing it through a 28-gauge insulin needle 10 times. Lysate equivalent to 10^5 cells was resolved using SDS/PAGE and transferred to a nitrocellulose membrane. The membrane was blocked in 5% milk in PBS with 0.1%Tween-20 and incubated with primary antibody in PBS/5% milk/0.1% Tween-20 for 2 hrs at room temperature. The following primary antibodies were utilized: TRF1 (1449, rabbit polyclonal); TRF2 (1254, rabbit polyclonal); Rap1 (1252, rabbit polyclonal); Chk2 (mouse monoclonal, BD Biosciences); Phospho-Chk1 (Ser 345) (mouse monoclonal, Cell Signaling); Chk1 (mouse monoclonal, Santa Cruz); BLM (rabbit polyclonal, Abcam); Lig3 (mouse monoclonal, Santa Cruz); PARP1 (mouse monoclonal, Millipore); CtIP (rabbit polyclonal, Santa Cruz H-300); Myc (9E10; Calbiochem); Flag (M2, sigma); γ- tubulin (clone GTU-88, Sigma).

In-gel analysis of single-stranded telomeric DNA

At the indicated time points, $1x10^6$ cells were harvested by trypsinization, suspended in PBS, mixed with 2% agarose (1:1 ratio) and casted in a plug mold. Plugs were digested overnight in proteinase K digestion buffer (10 mM Tris-HCl pH 8.0, 250 mM EDTA, 0.2% sodium deoxycholate, and 1% sodium lauryl sarcosine) at 55°C. After extensive washes with TE, plugs were incubated with 60U *Mbo*I and 60U *Alu*I overnight at 37°C. Treatment

with E. coli Exonuclease I was done prior to digestion with restriction enzymes. Agarose-embedded DNA plugs were washed 3 times with TE (1 hr each), once with water (1 hr) and twice with Exonuclease I buffer (67 mM Glycine-NaOH, 6.7 mM $MgCl_2$ and 10 mM 2-mercaptoethanol pH=9.5 at 25°C). Plugs were treated twice with 1000 U of Exonuclease I (NEB) in Exonuclease I buffer (12 hrs each) at 37°C. The plugs were then washed with TE, and digested with *Mbo*I and *Alu*I. Digested DNA was resolved on a 1% agarose/0.5XTBE gel by a CHEF-DRII PFGE apparatus (BioRad) for 24 hrs. The gels were then dried at room temperature and hybridized overnight at 50°C with γ-^{32}P-ATP end-labeled $[AACCCT]_4$ probe in Church mix (0.5 M sodium phosphate, pH 7.2, 1 mM EDTA, 0.7% SDS, 0.1% BSA). The gel was washed at 50°C three times in 4XSSC (30 min each), once in 4XSSC/0.1% SDS (30 min), and exposed to a PhosphoImager screen. After capturing the single-stranded telomere signal, the gel was denatured in situ with 0.5 M NaOH/1.5 M NaCl for 30 min, neutralized with two 30-min washes in 0.5 M Tris-HCl pH 7.5/3 M NaCl, prehybridized in Church mix for 30 min at 55°C, and hybridized overnight with the same probe at 55°C. The next day, the denatured gel was washed in the same way as the native gel and exposed to capture the total telomere signal. ImageQuant software was used to quantify the single-stranded telomere overhang signal and the signal from total telomeric DNA in the denatured gel.

FISH and Q-FISH

At the indicated time points, ~80% confluent MEFs were incubated for 2 hrs with 0.2 µg/ml colcemid (Sigma). The cells were harvested by trypsinization, resuspended in 0.075 M KCl at 37°C for 30 minutes, and fixed overnight in methanol/acetic acid (3:1) at 4°C. The cells were dropped onto glass slides in a Thermotron Cycler (20°C, 50% humidity) and the slides were dried overnight. The next day, the slides were rehydrated with PBS for 15 min then fixed with 4% formaldehyde for 2 min at room temperature. Slides were digested with 1 mg/ml Pepsin (pH 2.2) at 37°C for 10 minutes, washed three times with PBS and fixed again in 4% formaldehyde for 2 min at room temperature. After three PBS washes, the slides were incubated consecutively with 75%, 95%, and 100% ethanol and allowed to air dry for 30 min before applying hybridization solutions (70% formamide, 1 mg/ml blocking reagent (Roche), 10 mM Tris-HCl pH 7.2) containing FITC-OO-$[CCCTAA]_3$ or TAMRA-OO-$[TTAGGG]_3$ PNA probes (Applied Biosystems). Slides were denatured by heating for 3 min at 80°C and hybridized for 2 hrs at room temperature. Following hybridization, the slides were washed twice for 15 min each in

70% formamide/10 mM Tris-HCl, followed by three 5 min washes in 0.1 M Tris-HCl, pH 7.0/0.15 M NaCl/0.08% Tween-20. The chromosomal DNA was counterstained with 4,6-diamidino-2-phenylindole (DAPI) that was applied to the second wash. Slides were mounted in antifade reagent (ProLong Gold, Invitrogen) and digital images acquisition was done on a Zeiss Axioplan II microscope with a Hamamatsu C4742-95 camera using Improvision OpenLab software. Quantitative-FISH analysis was performed using TFL-Telo image analysis software as described by Poon et al., (*37*). Carboxylate-modified FluoSpheres (0.2 μM, Molecular Probes) were used for system calibration. Telomeres engaged in fusions and sister associations were excluded from Q-FISH analysis. Metaphase spreads from HeLa1.3 cells (*36*) were mixed with experimental samples and used as internal controls in one experiment.

CO-FISH

Cells were labeled with BrdU:BrdC (3:1, final concentration: 10 μM) for 14-16 hrs. 2 hrs prior to harvesting by trypsinization, 0.2 μg/ml colcemid was added to the media. To fix the cells and drop metaphases on a glass slide, the same procedure that was applied for FISH was followed. After drying the slides overnight, they were treated with 0.5 mg/ml RNase A (in PBS, DNase free) for 10 min at 37°C. The slides were incubated with 0.5 mg/ml Hoechst 33258 (Sigma) in 2XSSC for 15 min at room temperature followed by exposure to 365-nm UV light (Stratalinker 1800 UV irradiator) for 30 min. The slides were then digested twice with 800 U Exonuclease III (Promega) at room temperature for 10 min each, washed with PBS and dehydrated through an ethanol series of 70%, 95%, 100%. After air-drying, slides were hybridized with Tamra-OO-$[TTAGGG]_3$ PNA probe in hybridization solution (70% formamide, 1 mg/ml blocking reagent (Roche), 10 mM Tris-HCl pH 7.2) for 2 hrs at room temperature. The slides were then washed for few seconds with 70% formamide/10 mM Tris-HCl pH 7.2 and incubated with FITC-OO-$[CCCTAA]_3$ PNA probe in hybridization solution for 2 hrs. Slides were washed and mounted as described for FISH.

FACS

For cell cycle analysis, cells were incubated with 10 μM BrdU 2-4 hrs prior to harvesting. Cells were collected by trypsinization, washed in PBS, fixed with ice cold 70% ethanol and stained with FITC-conjugated anti-BrdU antibody (BD Biosciences) for 2 hrs at 37°C. Cells were then incubated with PI (propidium-iodide) and analyzed with a FACS calibur

flow cytometer (Becton Dickinson). Data was analyzed by FlowJo software.

FUCCI-FACS sorting

FUCCI-FACS sorting was done as previously described (*38*) using cells that were transduced by mKO2-Cdt1 30/120 and mAG-Geminin 1/110 lentiviral vectors.

MNase digestion

Analyzing nucleosomal configuration at telomeres was done using MNase digestion according to previously published protocols (*39, 40*)

Telomeric ChIP

Telomerc ChIP was performed as previously described (*41*). The following antibodies were used as crude sera: TRF1 (1449, rabbit polyclonal); TRF2 (1254, rabbit polyclonal); TIN2 (1447, rabbit polyclonal); Rap1 (1252, rabbit polyclonal); POT1a (1220, rabbit polyclonal); TPP1 (1150, rabbit polyclonal); POT1b (1223, rabbit polyclonal). The Myc (9E10, Calbiochem) and Flag (M2, Sigma) antibodies were used as provided by the manufacturer.

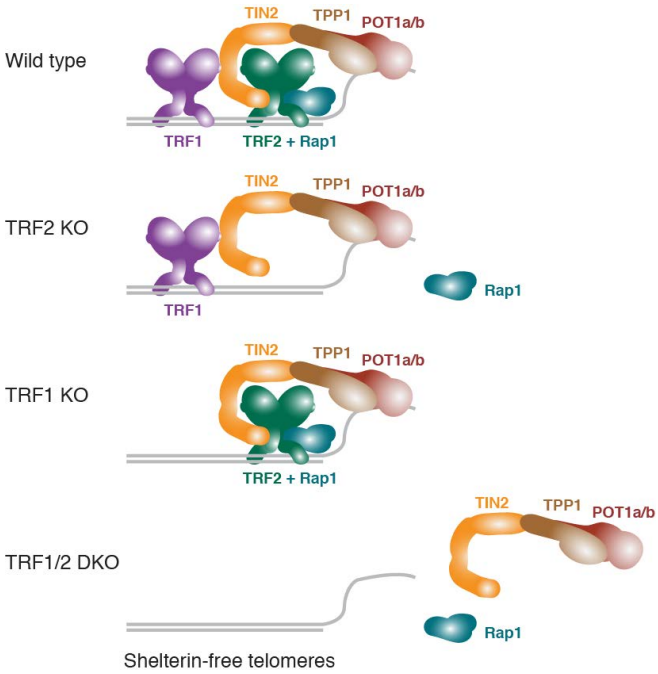

Fig. S1. Engineering shelterin-free telomeres. Schematic illustrating that either TRF1 or TRF2 can mediate the association of other shelterin components with telomeres. Co-deleting both double-stranded DNA binding proteins is expected to dislodge the remaining subunits from the TTAGGG repeats resulting in shelterin-free telomeres.

Figure S2. Sfeir and de Lange

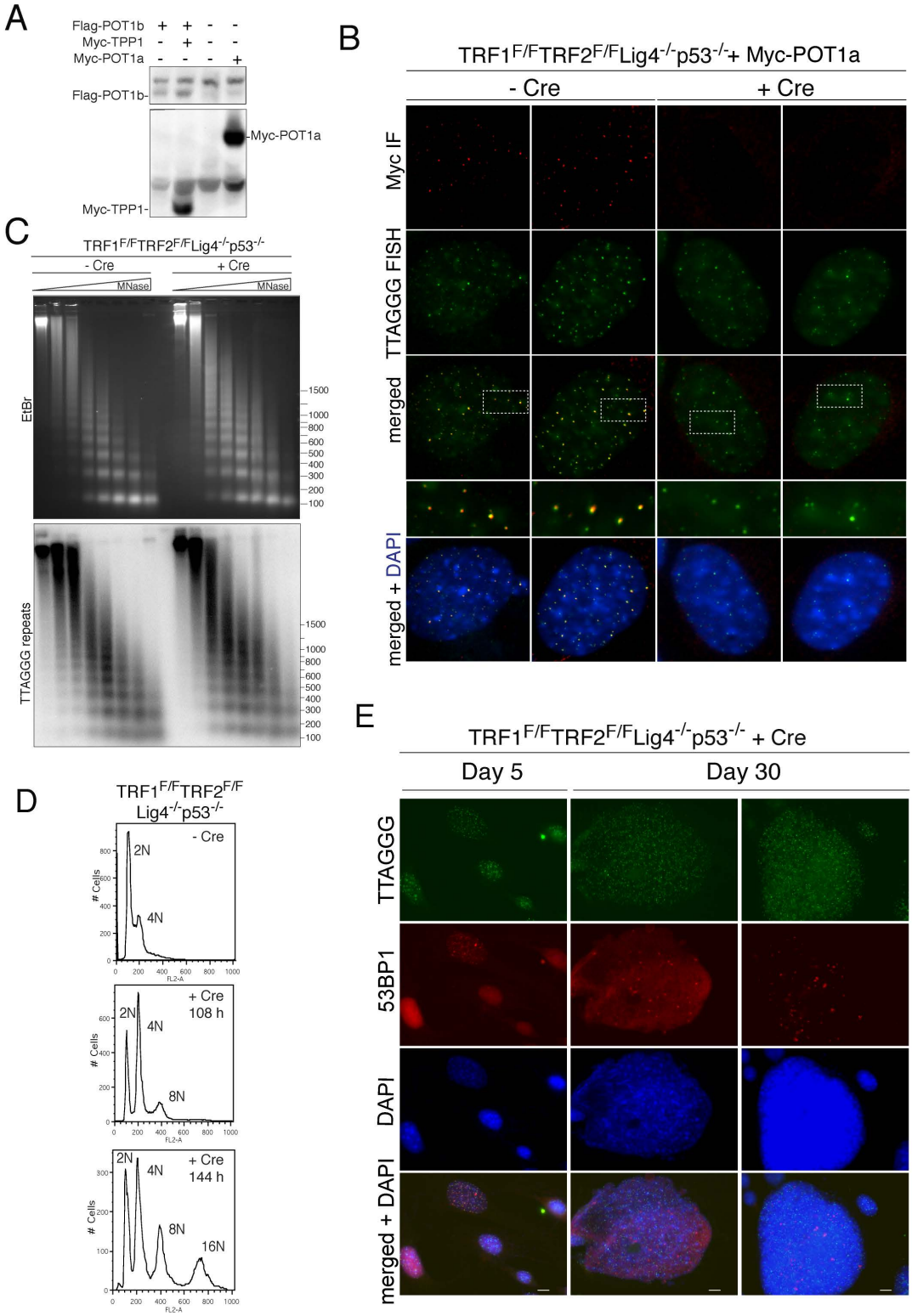

Fig. S2. Expression of tagged TPP1/POT allels and phenotypes of shelterin loss. (**A**) Immunoblots with Myc and Flag antibodies to monitor expression of Myc-POT1a, Myc-TPP1, and Flag-POT1b in TRF1$^{F/F}$TRF2$^{F/F}$Lig4$^{-/-}$p53$^{-/-}$ cells corresponding to experiments in Figure 1. **B**) IF for the telomeric localization of Myc-POT1a (Red) in TRF1$^{F/F}$TRF2$^{F/F}$p53$^{-/-}$Lig4$^{-/-}$ MEFs (5 days after H&R-Cre). Green: Telomeric PNA probe (**C**) Nucleosomal organization at telomeres is not affected by the deletion of TRF1 and TRF2. DNA from Micrococcal nuclease (MNase) digested nuclei of TRF1$^{F/F}$TRF2$^{F/F}$Lig4$^{-/-}$ p53$^{-/-}$ MEFs with and without Cre treatment was fractionated on a 1% agarose gel and stained with ethidium bromide (left panel) to detect bulk nucleosomes and then blotted and hybridized with a telomere-specific probe (right panel) to asses nucleosome structure of telomeric DNA. (**D**) Cell cycle profile based on FACS for DNA content (PI) after deletion of TRF1 and TRF2 from TRF1$^{F/F}$TRF2$^{F/F}$Lig4$^{-/-}$p53$^{-/-}$ MEFs at 108 and 144 hrs following treatment with H&R-Cre. Polyploidy is evident from the accumulation of cells with >4N DNA content in the Cre-treated samples. (**E**) Formation of large nuclei in TRF1$^{F/F}$TRF2$^{F/F}$Lig4$^{-/-}$p53$^{-/-}$ MEFs at the indicated time points after Cre treatment. Examples of enlarged nuclei with 53BP1 foci at telomeric DNA on day 30 after treatment with H&R-Cre. FISH for telomeres (green), IF for 53BP1 (red), and DAPI as DNA counterstain (blue). All images were captured at 40X (scale bar: 100 pixels).

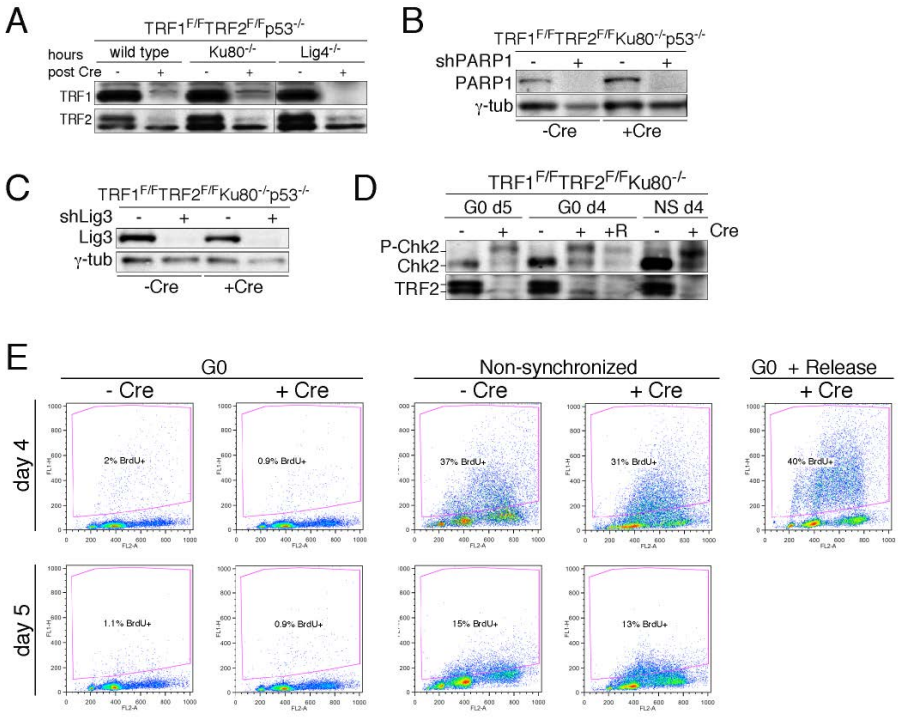

Fig. S3. Western and FACS analysis of Ku null cells after TRF1/2 DKO. (**A**) Immunoblot analysis for TRF1 and TRF2 in cells of the indicated genotypes at 108 hr after H&R Cre. (**B**) Western to monitor PARP1 protein levels in TRF1$^{F/F}$TRF2$^{F/F}$Ku80$^{-/-}$p53$^{-/-}$ cells with the indicated Cre and shRNA treatment. (**C**) Immunoblot for Lig3 in TRF1$^{F/F}$TRF2$^{F/F}$Ku80$^{-/-}$p53$^{-/-}$ cells with the indicated Cre and shRNA treatment. γ-tubulin serves as a loading control. (**D**) Western blot to monitor TRF2 levels and Chk2 phosphorylation in G0-arrested TRF1$^{F/F}$TRF2$^{F/F}$Ku80$^{-/-}$Cre-ER^{T2+} cells upon treatment with 4-OHT. (**E**) Cell cycle profile of TRF1$^{F/F}$TRF2$^{F/F}$Ku80$^{-/-}$Cre-ER^{T2+} cells at the time of telomere analysis by pulse-field gel electrophoresis in the experiment corresponding to Fig. 3E. Cells were pulsed with BrdU for 2 hrs prior to harvesting. Fixed cells were stained with FITC-anti-BrdU and propidium iodide (PI) for DNA content, and analyzed by flow cytometry. The percentage of BrdU positive cells is indicated within the FACS profile.

Figure S4. Sfeir and de Lange

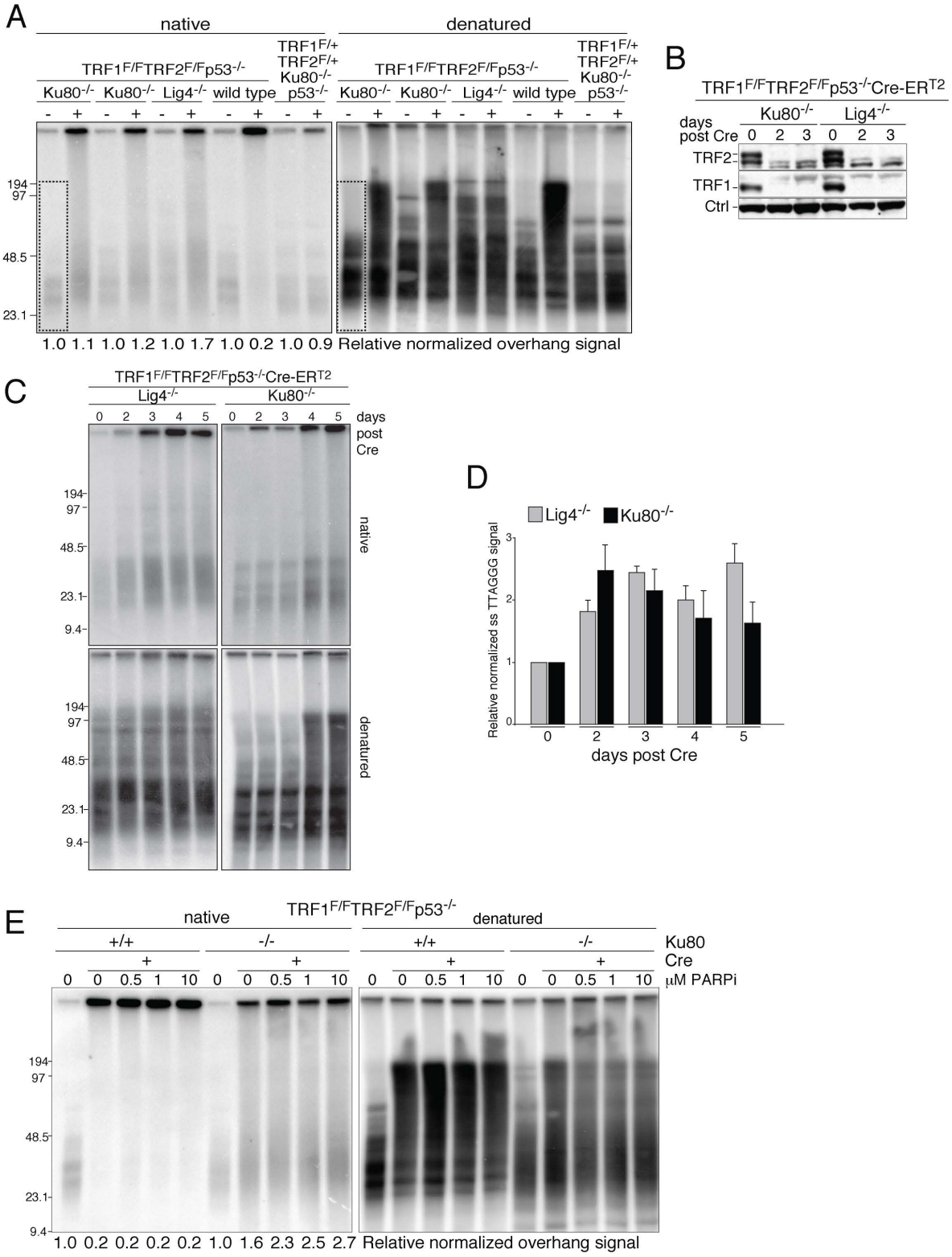

Fig. S4. Telomeric overhang signals after TRF1/2 co-deletion from Lig4 or Ku80 null MEFs. (**A**) Representative in-gel hybridization assay to assess 3' single-stranded telomeric overhang in MEFs of the indicated genotype with and without Cre infection. Left panel shows native 3' overhang signal. Right panel shows total telomere signal under denaturing conditions. Relative normalized signal was determined with the signal in the -Cre lane set to 1. The dashed box marks the region used to quantify the signal. (**B**) Western blot analysis for TRF1 and TRF2 in $TRF1^{F/F}$ $TRF2^{F/F}p53^{-/-}$ Cre-ER^{T2+} MEFs lacking either Ku80 or Lig4. Cre expression was induced with 4-OHT and cells were analyzed at the indicated time points. (**C**) Representative in-gel hybridization analysis of the 3' single-stranded telomeric 3'-overhang signal in MEFs with the indicated genotype and time course after deleting TRF1 and TRF2. Top: detection of the 3' overhang signal under native conditions. Bottom: detection of the total telomeric hybridization signal obtained after in situ denaturation of DNA and rehybridization to the same probe. (**D**) Quantification of the overhang analysis as assayed in (**C**). For each lane, the single stranded TTAGGG signal (top panel in C) was normalized to total telomeric signal (bottom panel in C). The single stranded/total signal ratio was set to 1 for the day 0 samples and the Cre treated samples are expressed relative to day 0. Values represent the mean of three independent experiments and SDs. (**E**) In-gel hybridization assay to assess 3' single-stranded telomere signal in $TRF1^{F/F}TRF2^{F/F}Ku80^{+/+}p53^{-/-}$ and $TRF1^{F/F}TRF2^{F/F}Ku80^{-/-}p53^{-/-}$ MEFs treated with increasing concentrations of olaparib. Cells were harvested at 108 hr following treatment with H&R Cre. Relative single-stranded TTAGGG signal in each lane was normalized to the total signal in the same lane of the denatured gel with the value in the - Cre lane set to 1.

A

TRF1$^{F/F}$TRF2$^{F/F}$ 53BP1$^{-/-}$p53$^{-/-}$		telomeres analyzed	telomere fusions
- Cre	+ Vector	820	0 %
- Cre	+ shLig3	730	0.5 %
+ Cre	+ Vector	1029	13.7%
+ Cre	+ shLig3	1106	5.6%

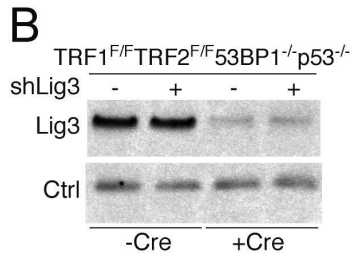

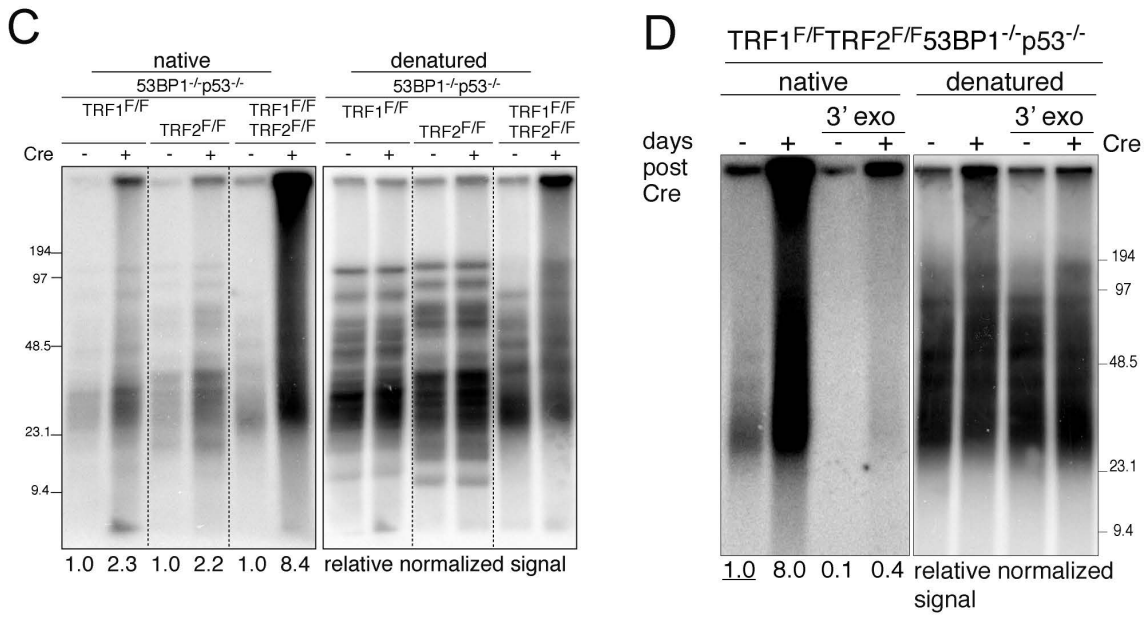

Fig. S5. Increased overhang signal in 53BP1 null cells appears upon loss of TRF1 and TRF2 and is sensitive to 3' exo. (**A**) Quantification of telomere fusions in Cre-treated TRF1$^{F/F}$TRF2$^{F/F}$53BP1$^{-/-}$p53$^{-/-}$ MEFs treated with shRNA for Lig3. (**B**) Immunoblot verifying Lig3 knockdown in TRF1$^{F/F}$TRF2$^{F/F}$53BP1$^{-/-}$p53$^{-/-}$ MEFs **(C**) 3' overhang assay of MEFs with the indicated genot2ype, analyzed at 108 hrs after infection with H&R Cre. (**D**) In-gel hybridization analysis of TRF1$^{F/F}$TRF2$^{F/F}$53BP1$^{-/-}$p53$^{-/-}$ MEFs with or without infection with Cre. DNA was treated with E. coli Exonucleas I to remove 3' terminal single stranded DNA prior to digestion with restriction enzymes. The relative normalized overhang signal was determined with the signal in the first lane (-Cre and - 3' exo) set to 1.

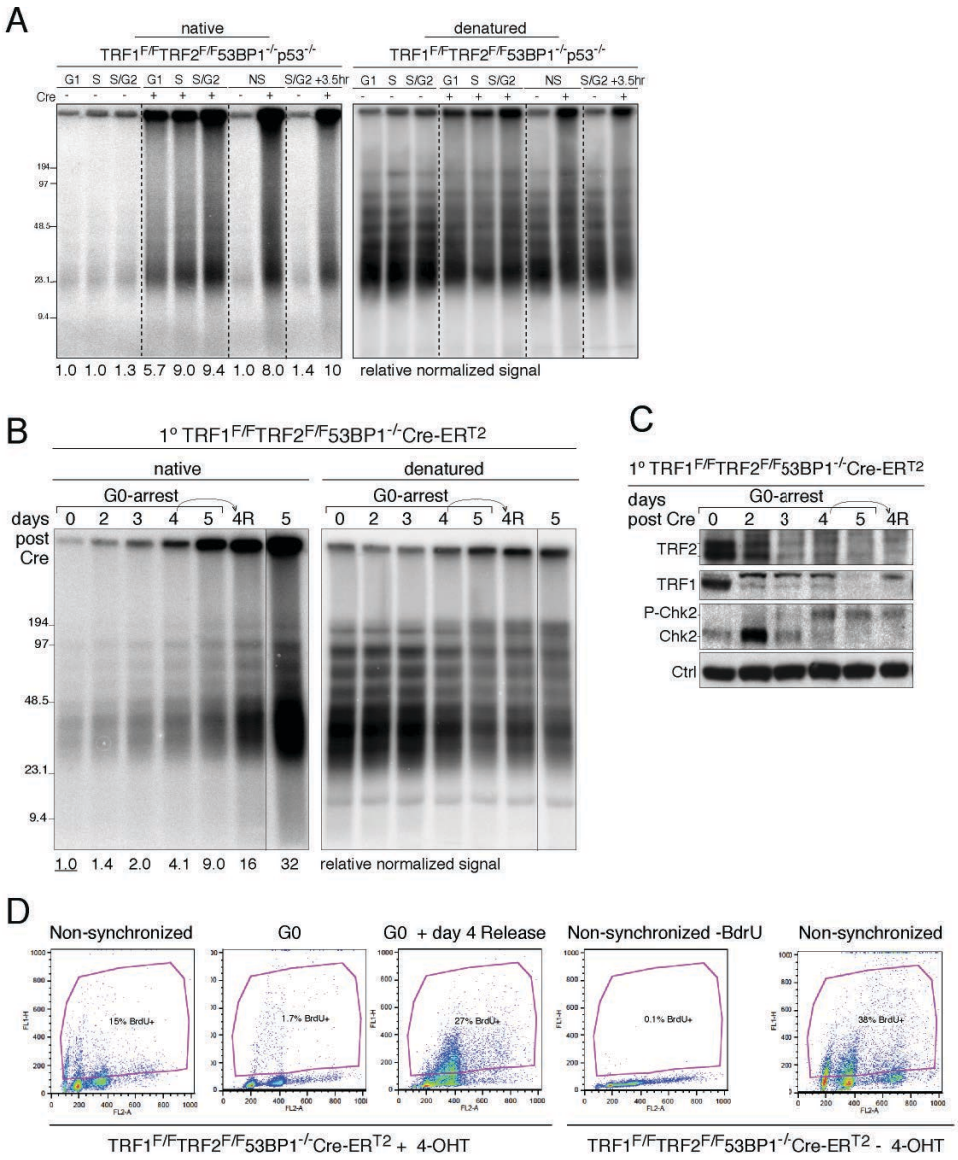

Fig. S6. Cell cycle effects on the increased overhang signal in TRF1/2 DKO 53BP1 cells. (**A**) Telomeric overhang analysis by in-gel hybridization of TRF1$^{F/F}$TRF2$^{F/F}$53BP1$^{-/-}$ p53$^{-/-}$ MEFs that are in G1, early S and late S/G2 phase of the cell cycle with or without H&R Cre-infection. FUCCI-FACS (*38*) was used to sort cells in different stages of the cell cycle. The relative normalized single-stranded telomere signal was determined with the signal in the lane corresponding to G1 without Cre set to 1. (**B**) In-gel 3' overhang assay on G0-arrested, released (4R), and asynchronous primary TRF1$^{F/F}$TRF2$^{F/F}$53BP1$^{-/-}$p53$^{+/+}$Cre-ER^{T2+} MEFs analyzed at the indicated days following 4-OHT treatment. Day 4R represents a Cre-treated sample that was released from G0 at day 4 and analyzed after 24 hrs. The relative normalized overhang signal was determined with the signal in

G0 cells at day 0 set to 1. (**C**) Western blot analysis for TRF1, TRF2, and Chk2 in G0 arrested TRF1$^{F/F}$TRF2$^{F/F}$53BP1$^{-/-}$p53$^{+/+}$Cre-ER^{T2+} MEFs shown in (**B**). (**D**) FACS profiles the cells used in (**B**). Cells were pulsed with BrdU for 4 hrs prior to harvesting and fixation for analysis by FACS. The percentage of BrdU positive cells is given within the FACS profile.

Figure S7. Sfeir and de Lange

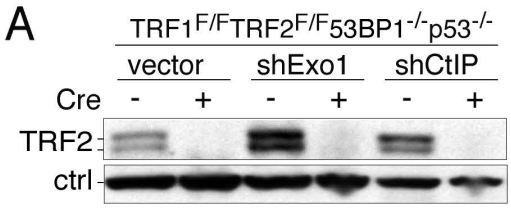

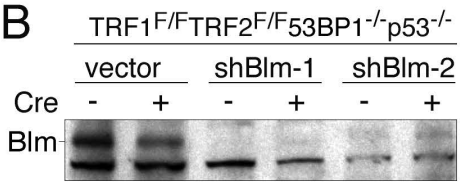

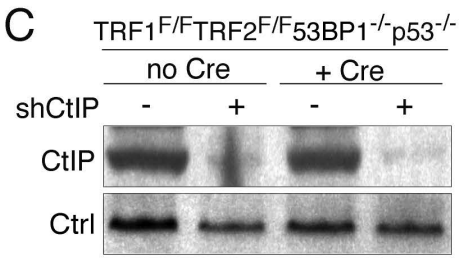

D

TRF1F/FTRF2F/F53BP1-/-p53-/- + Cre

	% BrdU positive
+ Vector	13.1
+ shExo1	9.7
+ shBlm1	17.3
+ shBlm2	11.5
+ shCtIP	9.64

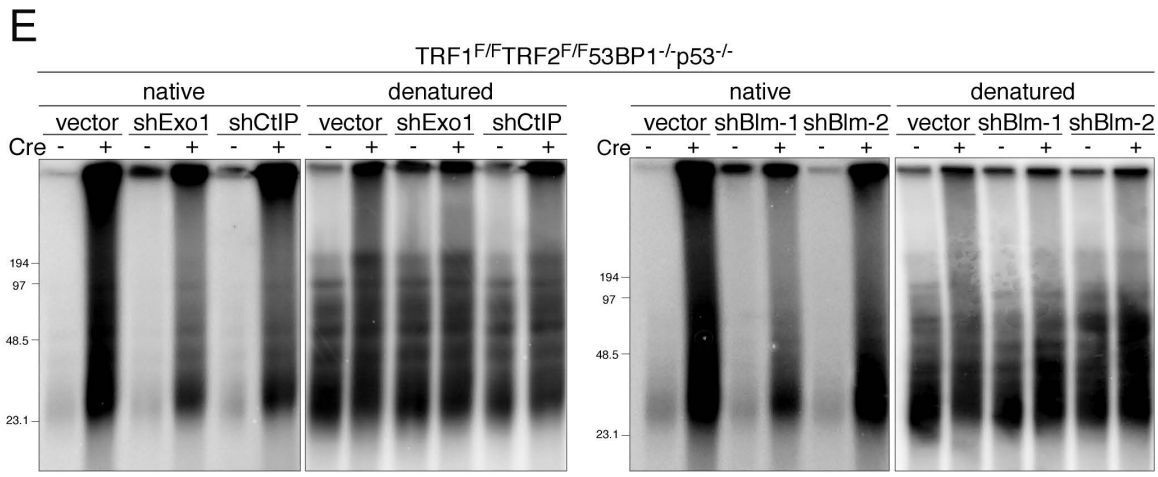

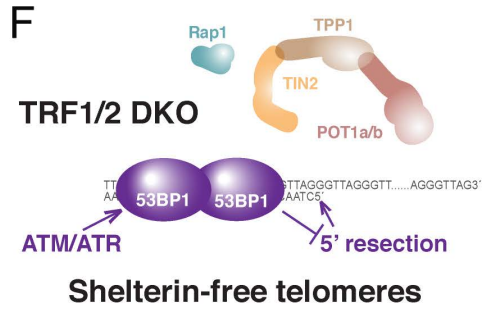

Fig. S7. 53BP1 protects shelterin-free telomeres from CtIP/Blm/Exo1 dependent resection. (**A**) Immunoblot verifying TRF2 deletion in $TRF1^{F/F}TRF2^{F/F}53BP1^{-/-}p53^{-/-}$ MEFs with the indicated shRNA and Cre treatment. (**B**) Immunoblot showing Blm knockdown in cells with the indicated shRNA and Cre treatment. (**C**) Immunoblot showing CtIP knockdown in cells with the indicated shRNA and Cre treatment. (**D**) The percentage of BrdU positive cells for Cre treated $TRF1^{F/F}TRF2^{F/F}53BP1^{-/-}p53^{-/-}$ MEFs with the indicated shRNA treatment at 4 days post Cre. Cells were pulsed with BrdU for 3 hrs prior to harvesting and fixation for analysis by FACS. (**E**) Representative in-gel 3' overhang assay on $TRF1^{F/F}TRF2^{F/F}53BP1^{-/-}p53^{-/-}$ MEFs (+ or - Cre) treated with Exo1, CtIP and Blm shRNA as indicated. MEFs were harvested at 108 hr following introduction of H&R Cre. (**F**) Summary of the protective role of 53BP1 at shelterin-free telomeres. In the absence of shelterin, ATM and ATR signaling at telomeres leads to accumulation of 53BP1, which inhibits 5' end resection by processing factors that act on DSBs.

References

1. T. de Lange, How telomeres solve the end-protection problem. *Science* **326**, 948 (2009). doi:10.1126/science.1170633 Medline

2. W. Palm, T. de Lange, How shelterin protects mammalian telomeres. *Annu. Rev. Genet.* **42**, 301 (2008). doi:10.1146/annurev.genet.41.110306.130350 Medline

3. G. B. Celli, T. de Lange, DNA processing is not required for ATM-mediated telomere damage response after TRF2 deletion. *Nat. Cell Biol.* **7**, 712 (2005). doi:10.1038/ncb1275 Medline

4. G. B. Celli, E. L. Denchi, T. de Lange, Ku70 stimulates fusion of dysfunctional telomeres yet protects chromosome ends from homologous recombination. *Nat. Cell Biol.* **8**, 885 (2006). doi:10.1038/ncb1444 Medline

5. N. Dimitrova, Y. C. Chen, D. L. Spector, T. de Lange, 53BP1 promotes non-homologous end joining of telomeres by increasing chromatin mobility. *Nature* **456**, 524 (2008). doi:10.1038/nature07433 Medline

6. E. L. Denchi, T. de Lange, Protection of telomeres through independent control of ATM and ATR by TRF2 and POT1. *Nature* **448**, 1068 (2007). doi:10.1038/nature06065 Medline

7. A. Sfeir *et al*., Mammalian telomeres resemble fragile sites and require TRF1 for efficient replication. *Cell* **138**, 90 (2009). doi:10.1016/j.cell.2009.06.021 Medline

8. P. Martínez *et al*., Increased telomere fragility and fusions resulting from TRF1 deficiency lead to degenerative pathologies and increased cancer in mice. *Genes Dev.* **23**, 2060 (2009). doi:10.1101/gad.543509 Medline

9. K. K. Takai, T. Kibe, J. R. Donigian, D. Frescas, T. de Lange, Telomere protection by TPP1/POT1 requires tethering to TIN2. *Mol. Cell* **44**, 647 (2011). doi:10.1016/j.molcel.2011.08.043 Medline

10. T. Kibe, G. A. Osawa, C. E. Keegan, T. de Lange, Telomere protection by TPP1 is mediated by POT1a and POT1b. *Mol. Cell. Biol.* **30**, 1059 (2010). doi:10.1128/MCB.01498-09 Medline

11. D. Hockemeyer, J. P. Daniels, H. Takai, T. de Lange, Recent expansion of the telomeric complex in rodents: Two distinct POT1 proteins protect mouse telomeres. *Cell* **126**, 63 (2006). doi:10.1016/j.cell.2006.04.044 Medline

12. A. Sfeir, S. Kabir, M. van Overbeek, G. B. Celli, T. de Lange, Loss of Rap1 induces telomere recombination in the absence of NHEJ or a DNA damage signal. *Science* **327**, 1657 (2010). doi:10.1126/science.1185100 Medline

13. W. Palm, D. Hockemeyer, T. Kibe, T. de Lange, Functional dissection of human and mouse POT1 proteins. *Mol. Cell. Biol.* **29**, 471 (2009). doi:10.1128/MCB.01352-08 Medline

14. C. Boboila *et al*., Alternative end-joining catalyzes class switch recombination in the absence of both Ku70 and DNA ligase 4. *J. Exp. Med.* **207**, 417 (2010). doi:10.1084/jem.20092449 Medline

15. R. Rai *et al*., The function of classical and alternative non-homologous end-joining pathways in the fusion of dysfunctional telomeres. *EMBO J.* **29**, 2598 (2010). doi:10.1038/emboj.2010.142 Medline

16. M. Wang *et al*., PARP-1 and Ku compete for repair of DNA double strand breaks by distinct NHEJ pathways. *Nucleic Acids Res.* **34**, 6170 (2006). doi:10.1093/nar/gkl840 Medline

17. D. Simsek, M. Jasin, Alternative end-joining is suppressed by the canonical NHEJ component Xrcc4-ligase IV during chromosomal translocation formation. *Nat. Struct. Mol. Biol.* **17**, 410 (2010). doi:10.1038/nsmb.1773 Medline

18. C. T. Yan *et al*., IgH class switching and translocations use a robust non-classical end-joining pathway. *Nature* **449**, 478 (2007). doi:10.1038/nature06020 Medline

19. W. Y. Mansour, T. Rhein, J. Dahm-Daphi, The alternative end-joining pathway for repair of DNA double-strand breaks requires PARP1 but is not dependent upon microhomologies. *Nucleic Acids Res.* **38**, 6065 (2010). doi:10.1093/nar/gkq387 Medline

20. K. A. Menear *et al*., 4-[3-(4-cyclopropanecarbonylpiperazine-1-carbonyl)-4-fluorobenzyl]-2H-phthalazin-1-one: a novel bioavailable inhibitor of poly(ADP-ribose) polymerase-1. *J. Med. Chem.* **51**, 6581 (2008). doi:10.1021/jm8001263 Medline

21. D. Simsek *et al*., DNA ligase III promotes alternative nonhomologous end-joining during chromosomal translocation formation. *PLoS Genet.* **7**, e1002080 (2011). doi:10.1371/journal.pgen.1002080 Medline

22. P. Baumann, T. R. Cech, Protection of telomeres by the Ku protein in fission yeast. *Mol. Biol. Cell* **11**, 3265 (2000). Medline

23. S. Gravel, M. Larrivée, P. Labrecque, R. J. Wellinger, Yeast Ku as a regulator of chromosomal DNA end structure. *Science* **280**, 741 (1998). doi:10.1126/science.280.5364.741 Medline

24. R. M. Polotnianka, J. Li, A. J. Lustig, The yeast Ku heterodimer is essential for protection of the telomere against nucleolytic and recombinational activities. *Curr. Biol.* **8**, 831 (1998). doi:10.1016/S0960-9822(98)70325-2 Medline

25. K. Riha, D. E. Shippen, Ku is required for telomeric C-rich strand maintenance but not for end-to-end chromosome fusions in Arabidopsis. *Proc. Natl. Acad. Sci. U.S.A.* **100**, 611 (2003). doi:10.1073/pnas.0236128100 Medline

26. P. Bouwman *et al*., 53BP1 loss rescues BRCA1 deficiency and is associated with triple-negative and BRCA-mutated breast cancers. *Nat. Struct. Mol. Biol.* **17**, 688 (2010). doi:10.1038/nsmb.1831 Medline

27. S. F. Bunting *et al*., 53BP1 inhibits homologous recombination in Brca1-deficient cells by blocking resection of DNA breaks. *Cell* **141**, 243 (2010). doi:10.1016/j.cell.2010.03.012 Medline

28. E. P. Mimitou, L. S. Symington, Sae2, Exo1 and Sgs1 collaborate in DNA double-strand break processing. *Nature* **455**, 770 (2008). doi:10.1038/nature07312 Medline

29. Z. Zhu, W. H. Chung, E. Y. Shim, S. E. Lee, G. Ira, Sgs1 helicase and two nucleases Dna2 and Exo1 resect DNA double-strand break ends. *Cell* **134**, 981 (2008). doi:10.1016/j.cell.2008.08.037 Medline

30. S. Gravel, J. R. Chapman, C. Magill, S. P. Jackson, DNA helicases Sgs1 and BLM promote DNA double-strand break resection. *Genes Dev.* **22**, 2767 (2008). doi:10.1101/gad.503108 Medline

31. T. Jacks *et al*., Tumor spectrum analysis in p53-mutant mice. *Curr. Biol.* **4**, 1 (1994). doi:10.1016/S0960-9822(00)00002-6 Medline

32. A. Ventura *et al*., Restoration of p53 function leads to tumour regression in vivo. *Nature* **445**, 661 (2007). doi:10.1038/nature05541 Medline

33. K. M. Frank *et al*., Late embryonic lethality and impaired V(D)J recombination in mice lacking DNA ligase IV. *Nature* **396**, 173 (1998). doi:10.1038/24172 Medline

34. I. M. Ward, K. Minn, J. van Deursen, J. Chen, p53 Binding protein 53BP1 is required for DNA damage responses and tumor suppression in mice. *Mol. Cell. Biol.* **23**, 2556 (2003). doi:10.1128/MCB.23.7.2556-2563.2003 Medline

35. A. Nussenzweig *et al*., Requirement for Ku80 in growth and immunoglobulin V(D)J recombination. *Nature* **382**, 551 (1996). doi:10.1038/382551a0 Medline

36. H. Takai, A. Smogorzewska, T. de Lange, DNA damage foci at dysfunctional telomeres. *Curr. Biol.* **13**, 1549 (2003). doi:10.1016/S0960-9822(03)00542-6 Medline

37. S. S. Poon, P. M. Lansdorp, *Curr. Protoc. Cell Biol.*, Chapter 18, Unit 18.4 (2001).

38. P. Wu, M. van Overbeek, S. Rooney, T. de Lange, Apollo contributes to G overhang maintenance and protects leading-end telomeres. *Mol. Cell* **39**, 606 (2010). doi:10.1016/j.molcel.2010.06.031

39. H. Tommerup, A. Dousmanis, T. de Lange, Unusual chromatin in human telomeres. *Mol. Cell. Biol.* **14**, 5777 (1994). doi:10.1128/MCB.14.9.5777 Medline

40. P. Wu, T. de Lange, No overt nucleosome eviction at deprotected telomeres. *Mol. Cell. Biol.* **28**, 5724 (2008). doi:10.1128/MCB.01764-07 Medline

41. D. Loayza, T. de Lange, POT1 as a terminal transducer of TRF1 telomere length control. *Nature* **423**, 1013 (2003). doi:10.1038/nature01688